Editors' Suggestion

Moiré Landau Fans and Magic Zeros

Nisarga Paul,* Philip J. D. Crowley,* Trithep Devakul,* and Liang Fu
Department of Physics, Massachusetts Institute of Technology, Cambridge, Massachusetts 02139, USA

(Received 24 February 2022; accepted 23 August 2022; published 9 September 2022; corrected 27 July 2023)

We study the energy spectrum of moiré systems under a uniform magnetic field. The superlattice potential generally broadens Landau levels into Chern bands with finite bandwidth. However, we find that these Chern bands become flat at a discrete set of magnetic fields which we dub "magic zeros." The flat band subspace is generally different from the Landau level subspace in the absence of the moiré superlattice. By developing a semiclassical quantization method and taking account of superlattice induced Bragg reflection, we prove that magic zeros arise from the simultaneous quantization of two distinct k-space orbits. For instance, we show the chiral model of TBG has flat bands at special fields for *any* twist angle in the nth Landau level for $|n| > 1$. The flat bands at magic zeros provide a new setting for exploring crystalline fractional quantum Hall physics.

DOI: 10.1103/PhysRevLett.129.116804

The advent of moiré materials has opened a new regime for the study of Bloch electrons under a magnetic field [1–5]. Moiré materials feature a superlattice period that is much larger than the atomic spacing and can be comparable to the magnetic length at $B = 1$ T (26 nm). Moreover, the superlattice potential that creates minibands is weak and slowly varying. As a result of both features, the interplay between Landau quantization and superlattice potential can give rise to a complex energy spectrum and novel quantum phenomena not found in ordinary solids [6–14].

In this work, we study the energy spectrum of two-dimensional moiré materials under a magnetic field B. Our work mainly focuses on the case of a superlattice potential not too strong relative to bandwidth such that the corresponding moiré bands can be treated by nearly free electron approximation. The energy spectrum as a function of magnetic field displays three distinct regimes. At very small magnetic fields, a set of Landau levels (LLs) arise from the standard semiclassical quantization [15] of cylotron orbits that follow the constant energy contour of moiré bands. In the opposite limit of very large fields, a different set of LLs which come from "free" electrons without moiré effects are recovered. In the wide range of intermediate magnetic fields, the competition between magnetic breakdown and superlattice induced Bragg reflection at the mini Brillouin zone boundary leads to a new type of energy spectrum with remarkable universal features, which is the main finding of this work.

We develop a general method to calculate the Landau spectrum on the moiré superlattice. We show that at intermediate magnetic fields, the LLs of free electrons are generally broadened by Bragg scattering off the moiré superlattice, or in a complementary way, the LLs of Bloch electrons are broadened by magnetic breakdown near the mini Brillouin zone boundary. Remarkably, flat bands are found at a discrete set of magnetic fields, which we dub "magic zeros." Plotted in the (B, μ) plane, where μ is the chemical potential, each zero occurs at the intersection of two fictitious LL fans, corresponding to the simultaneous quantization of two distinct k-space orbits. The corresponding density of states divergence predicted by our theory directly manifests as a peak in the compressibility $dn/d\mu$. Alternatively, LL widths can be measured directly by STM [12] and inferred from inter-LL optical transitions [16]. One application is chiral twisted bilayer graphene (TBG), which we find has magic zeros in LLs for $|n| > 1$ at *all* twist angles and not just the discrete set of magic angles [17].

Importantly, we show the existence of these flat bands is robust and not limited to the particular known case of Schrödinger or Dirac LLs perturbed by a weak potential $V_0 \ll \omega_c$ (with ω_c the cyclotron frequency) [18]. In contrast, our theory of magic zeros is nonperturbative in V_0/ω_c and applicable to generic energy dispersions. We show the flat band at a magic zero spans a Hilbert space that is generally distinct from the LL subspace of free electrons. The physics of flat bands at magic zeros contrasts and complements the broadening and Hofstadter-type splitting of LLs at generic B fields.

We consider a two-dimensional Bloch electron in a uniform magnetic field

$$H = H_0(\boldsymbol{p} - e\boldsymbol{A}) + V(\boldsymbol{r}), \tag{1}$$

where $H_0(\boldsymbol{p})$ denotes the energy dispersion in the absence of the moiré superlattice and $\boldsymbol{A}$ is the vector potential.

$$V(\boldsymbol{r}) = \sum_{\boldsymbol{q}} V(\boldsymbol{q}) e^{i\boldsymbol{q}\cdot\boldsymbol{r}} + \text{c.c.} \tag{2}$$

denotes a periodic moiré potential ($\hbar = 1$). As the superlattice potential in moiré materials is slowly varying, $V(\boldsymbol{r})$

TABLE I. Values of ql_B for which the nth LL has zero bandwidth for weak potential, where q is the potential wave vector and l_B the magnetic length, for Schrödinger and Dirac electrons. The nth level exhibits $|n|$ magic zeros.

$\|n\|$	ql_B (Schrödinger case)	ql_B (Dirac case)
1	$\sqrt{2}$	2
2	1.08, 2.61	1.24, 3.24
3	0.91, 2.14, 3.55	0.99, 2.36, 4.18
4	0.80, 1.87, 3.01, 4.34	0.86, 2, 3.26, 4.96
5	0.73, 1.68, 2.68, 3.77, 5.03	0.76, 1.77, 2.84, 4.03, 5.65

is well approximated as a sum of a few lowest leading harmonics.

Depending on the form of H_0 and V, H describes a wide variety of moiré materials. In the case of semiconductor transition metal dichalcogenide (TMD) heterostructures such as WSe_2/WS_2, $H_0(\boldsymbol{p}) = p^2/2m$ where m is the effective mass near the band edge of TMD monolayer, and the triangular symmetric potential $V(\boldsymbol{r})$ is composed of three Fourier components of equal magnitude at wave vectors related by symmetry [19]. In the case of graphene on a one-dimensional patterned dielectric superlattice, $H_0(\boldsymbol{p}) = v\boldsymbol{p}\cdot\sigma$ is the Dirac Hamiltonian of graphene, and $V(\boldsymbol{r}) = V_0\cos(qx)$ involves a single wave vector only [6]. In both cases, the periodic potential $V(\boldsymbol{r})$ results in minibands, as manifested in resistive peaks at commensurate densities. Under a magnetic field, transport measurements observed complex patterns in the LL spectra.

The first indication of magic zeros can be found in the regime where the superlattice potential strength is smaller than the cyclotron energy ω_c of free electrons [18]. In this perturbative regime, $V(\boldsymbol{r})$ lifts the infinite degeneracy within a LL. The projection of periodic potential into the nth LL of Schrödinger electrons can then be written [18,20] (choosing symmetric gauge $\boldsymbol{A} = \frac{1}{2}\boldsymbol{B}\times\boldsymbol{r}$)

$$V_n^{\mathrm{eff}} = \sum_{\boldsymbol{q}} V(\boldsymbol{q}) e^{-q^2 l_B^2/4} L_n(q^2 l_B^2/2) e^{i\boldsymbol{q}\cdot(-\tilde{\pi}_y,\tilde{\pi}_x)l_B^2}, \quad (3)$$

where $l_B = 1/\sqrt{eB}$ is the magnetic length, $\tilde{\boldsymbol{\pi}} = \boldsymbol{p} + e\boldsymbol{A}$, and L_n is the nth Laguerre polynomial. Note $[\tilde{\pi}_x, \tilde{\pi}_y] = -ieB$. Notably, when all wave vectors are of equal magnitude q, the LL projected potential in Eq. (3) vanishes at n values of ql_B due to the Laguerre polynomial zeros, leading to a flat Chern band despite the presence of periodic potential. In the case of Dirac electrons, the nth LL wave function is a two-component spinor and the projected potential is given by [21] $\tilde{V}_n^{\mathrm{eff}} = (V_{|n|}^{\mathrm{eff}} + V_{|n|-1}^{\mathrm{eff}})/2$ for $n \neq 0$. Zeros occur in this case as well. Magic zeros for the first few LLs are listed in Table I, and the perturbative spectrum for a sixfold symmetric potential is shown in Figs. 1(c) and 1(d).

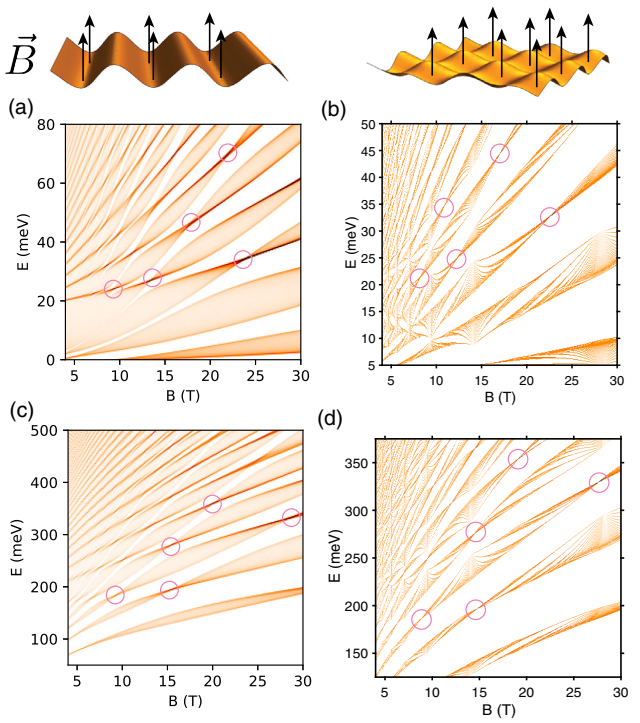

FIG. 1. DOS in a periodic potential and magnetic field for Schrödinger (a),(c) and Dirac (b),(d) electrons. A few prominent magic zeros are circled, robust features where the bandwidth vanishes. (a),(b) Exact diagonalization for a 1D periodic potential. (c),(d) Perturbative results for a 2D sixfold symmetric potential. Parameters: (a) $V_0 = 15$ meV, $m^* = 0.2m_e$, (b) $V_0 = 70$ meV, $v = 10^6$ m/s, (c) $V_0 = 4$ meV, $m^* = 0.2m_e$, (d) $V_0 = 25$ meV, $v = 10^6$ m/s. Period $a = 13$ nm.

Remarkably, we find that the magic zeros persist beyond the perturbative regime, as indicated by the exact diagonalization (ED) of the energy spectrum of Eq. (1) in Figs. 1(a) and 1(b) for the case of a potential $V_0\cos(qx)$. At the density of states (DOS) peaks shown, the bandwidth is zero within numerical accuracy, even in the regime $V_0/\omega_c \sim 3$. This result is truly all-orders in V_0/ω_c, as indicated by the following: (i) magic zeros deviate from the Laguerre polynomial zeros and (ii) the wave function at the zeros differs from the LL wave function at $V(\boldsymbol{r}) = 0$ (see Supplemental Material [22]).

In order to uncover the origin of these zeros, we develop a semiclassical approach which places no restrictions on V_0/ω_c. Moreover, this approach does not rely on a specific form of energy dispersion $H_0(\boldsymbol{p})$, and thus is applicable to a wider range of systems, such as bilayer graphene with trigonal warping. The starting point for the semiclassics is to consider a Bloch wave packet whose position and momentum are governed by the equations

$$\dot{\boldsymbol{p}} = -e\dot{\boldsymbol{r}}\times\boldsymbol{B}, \qquad \dot{\boldsymbol{r}} = \nabla E(\boldsymbol{p}), \quad (4)$$

where $E(\boldsymbol{p})$ is the energy dispersion *including* the effect of the periodic potential.

When the potential $V(\boldsymbol{r})$ is absent, electrons at an energy ε follow the original Fermi surface $H_0(\boldsymbol{p}) = \varepsilon$. When the potential is strong, electrons follow the reconstructed Fermi surface $E(\boldsymbol{p}) = \varepsilon$ where $\boldsymbol{p}$ lies in the mini Brillouin zone. In both cases, semiclassical quantization predicts infinitely degenerate LLs whenever the real-space orbits, which are simply $\boldsymbol{p}$-space orbits rotated by $\pi/2$ and scaled by $1/B$, enclose integer flux [15].

In between these two limits, magnetic breakdown [23–25] broadens the LLs. Let us consider an intersection of two original Fermi surfaces at the first Bragg plane in the repeated-zone scheme. In a magnetic field, there are two incoming and two outgoing electron wave packets. Thus we may treat the intersection as a two-level Landau-Zener system with a scattering matrix U. When B is sufficiently small, electrons follow on the reconstructed Fermi surface and occasionally breakthrough, and U is mainly diagonal. When B is large, electrons follow the original Fermi surface and occasionally Bragg scatter, so U is mainly off-diagonal.

In general, the scattering matrix takes the form

$$U = \begin{pmatrix} \sqrt{1-P}e^{-i\tilde{\varphi}_S} & -\sqrt{P} \\ \sqrt{P} & \sqrt{1-P}e^{i\tilde{\varphi}_S} \end{pmatrix}, \tag{5}$$

where the magnetic breakdown probability is

$$P = e^{-2\pi/\delta}, \qquad \delta = 16eBv_1v_2\sin\alpha/E_{\mathrm{gap}}^2; \tag{6}$$

$\boldsymbol{v}_1$ and $\boldsymbol{v}_2$ are incoming electron velocities which differ by an angle α, $E_{\mathrm{gap}} = 2V_0$ is the band gap at the Bragg plane, and $\tilde{\varphi}_S = \varphi_S - \pi/2$ with $\varphi_S = \pi/4 - (\ln\delta + 1)/\delta + \arg\Gamma(1 - i/\delta)$, the so-called Stokes phase [23,26] (see Supplemental Material [22]). We note $e^{-i\tilde{\varphi}_S}$ only depends weakly on δ, interpolating between i and $i^{1/2}$. Equations (5) and (6) are derived using the nearly free electron approximation assuming that the effect of the potential on the band structure is only significant near the Brillouin zone boundary. Note that P goes to zero quickly at low fields and approaches 1 at high fields.

In the case of parabolic bands, δ reduces to $8\varepsilon\omega_c\sin\alpha/V_0^2$. For bilayer TMDs with $\varepsilon \sim 20$ to 40 meV, $q \sim k_F$ (k_F is the Fermi wave vector), and $\omega_c \sim 2$ meV at 10 T, $P \sim 0.1$ to 0.3. For graphene in a 1D potential [6], taking $V_0 a/v_F \sim 1$ to 10, $a \sim 50$ nm, $q \sim k_F$, and $B \sim 10$ T gives $P \sim 0.01$ to 0.95. Evidently, realistic values of P in moiré materials require that the effects of magnetic breakdown are properly taken into account.

To properly account for magnetic breakdown, we consider a network model comprised of the original Fermi surfaces in the repeated zone scheme where wave packet motion away from the intersections is free-electron-like while scattering at the intersections is given by the Landau-Zener unitary U. Let us first consider networks in which the neighboring Fermi surface intersects at two points as in Fig. 2(a). This is similar in spirit to models considered by

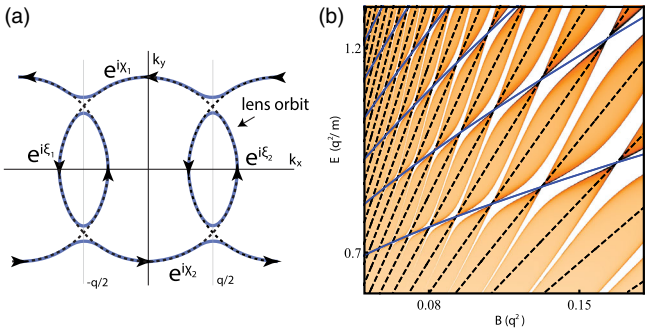

FIG. 2. (a) Fermi surface in the repeated zone scheme in the presence of a 1D potential $V_0\cos(qx)$. The network model (dashed lines) involves scattering at intersections and phases picked up on links. (b) Intersecting Landau fans due to the original orbit (dashed lines) and lens orbit (blue), and semiclassical DOS (density plot) with $V_0 = 0.4$, $q = 2$, $m = 1$.

Pippard [27,28]; we refer to [29–31] for other examples of network model constructions. We refer to the original Fermi surfaces defined by $H_0(\boldsymbol{p}) = \varepsilon$ as the "original orbit" and their intersection as the "lens orbit."

To understand the magic zero condition in the semiclassical approach, it is instructive to consider the scattering matrix across a lens orbit, which is given by

$$W = \frac{1}{(1-P)e^{i(\xi_1+\xi_2+2\tilde{\varphi}_S)} - 1}\begin{pmatrix} Pe^{i\xi_1} & \kappa \\ \kappa & Pe^{i\xi_2} \end{pmatrix}, \tag{7a}$$

$$\kappa = e^{-i\tilde{\varphi}_S}\sqrt{1-P}(e^{i(\xi_1+\xi_2+2\tilde{\varphi}_S)} - 1), \tag{7b}$$

where ξ_1, ξ_2 are the phases acquired along the links of the lens orbit. W describes scattering between incoming and outgoing states across the lens orbit. When W is diagonal, incoming states scatter into outgoing states in the same zone.

We note that when $\xi_1 + \xi_2 + 2\tilde{\varphi}_S$ is an integer multiple of 2π, W is diagonal, indicating the decoupling of neighboring orbits in the network. This is reminiscent of constructive interference in a Fabry-Pérot optical cavity [8,32], where the lens orbit plays the role of the cavity. The decoupled orbits are valid eigenstates when the phase around the original orbit is an integer multiple of 2π. Under these conditions, the network model supports an extensive set of states which are localized and dispersionless, i.e., a flat band.

In brief, the flat band conditions, in terms of the phases shown in Fig. 2(a), are $\sum\xi_i + 2\tilde{\varphi}_S \in 2\pi\mathbb{Z}$ and $\sum(\xi_i + \chi_i) \in 2\pi\mathbb{Z}$. The phases satisfy

$$\sum_{\mathrm{orig.}}\xi_i + \chi_i = l_B^2 S_0 + 2\pi\gamma, \qquad \sum_{\mathrm{lens}}\xi_i = l_B^2 S_1 + 2\pi\gamma, \tag{8}$$

where S_0, S_1 are the $\boldsymbol{p}$-space areas of the original and lens orbits, respectively. We have added the topological Maslov contribution $\gamma = 1/2 - \varphi_{\mathrm{Berry}}/2\pi$ which is customary in

semiclassical treatments for closed orbits deformable to a circle [33–36], with Schrödinger and Dirac electrons having $\gamma = 1/2$ and 0, respectively. φ_{Berry} is the Berry phase along the orbit.

Combining the above conditions, we find that bandwidth zeros occur at the intersection of the two Landau fans given by

$$l_B^2 S_0 = 2\pi(n+\gamma), \tag{9a}$$

$$l_B^2 S_1 = 2\pi(m+\gamma-\tilde{\varphi}_S/\pi), \tag{9b}$$

for suitable integers m, n. These equations stipulate that both the original and lens orbits enclose integer flux, up to the Stokes phase and Maslov correction. The magic zero conditions, i.e., Eq. (9), can be roughly thought of as Bohr-Sommerfeld quantization conditions for both the original and lens orbits. In general, a sufficient condition for magic zeros is a Fermi contour with only *two* relevant independent semiclassical electron orbits (with other orbit areas integer linear combinations of these). For circular Fermi surfaces, these two areas are

$$S_0 = \pi k_F^2, \qquad S_1 = 2k_F^2(\cos^{-1}x - x\sqrt{1-x^2}), \tag{10}$$

where $x = q/2k_F$. For this case the intersecting Landau fans are shown in Fig. 2(b).

In the large n and weak potential limit, the semiclassical and perturbative approaches are expected to agree. Equation (10) and Eq. (9a) give $k_F^2 = 2(n+\gamma)/l_B^2$. Applying this to Eqs. (9b) and (10) and noting $\tilde{\varphi}_S/\pi \to -1/4$ at weak potential, the values of ql_B at which the nth LL has a magic zero are given by

$$ql_B = \frac{\pi(n-m-1/4)}{\sqrt{2n}} + O(n^{-1}) \tag{11}$$

for integers m, n. In the perturbative regime, Eq. (3) implies that these are the zeros of $L_n(q^2l_B^2/2)$. Indeed, by applying the large n formula [37]

$$e^{-\frac{q^2l_B^2}{4}} L_n(q^2l_B^2/2) = \frac{\cos(\sqrt{2n}ql_B - \frac{\pi}{4})}{\sqrt{\pi ql_B\sqrt{n/2}}} + O(n^{-\frac{3}{4}}), \tag{12}$$

we see that these magic zero conditions derived independently are identical. We remark that the phenomenon of Weiss oscillations [8,18,38–41]—superlattice induced magnetoresistance oscillations—is naturally captured by the semiclassical approach in this regime (see Supplemental Material [22]).

So far we have only discussed magic zeros, but the network model also allows us to calculate the band dispersion at generic fields using a transfer matrix approach. For the network in Fig. 2 due to a 1D potential (we defer discussion of the 2D case), the transfer matrix eigenvalues $e^{\pm i\theta}$ satisfy the relation

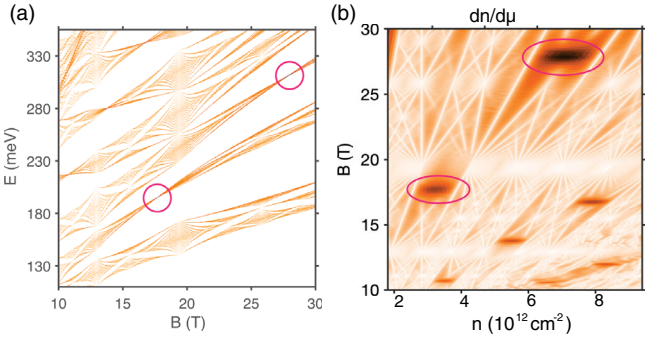

FIG. 3. (a) DOS for chiral limit TBG with $V_0 = 30$ meV, $v = 10^6$ m/s at $\theta = 1.1°$. Zeros exist at any twist angle. (b) Noninteracting compressibility as a function of density and B at $T = 0.2$ meV. Magic zeros are dark features of high compressibility occurring over a finite range of n.

$$\cos\theta = \frac{\sin(\xi+\chi) + (1-P)\sin(\xi-\chi+2\tilde{\varphi}_S)}{2\sqrt{1-P}\sin(\xi+\tilde{\varphi}_S)}, \tag{13}$$

where a gauge choice such that $\xi_1 = \xi_2 = \xi$ and $\chi_1 = \chi_2 = \chi$ has been made. The resulting semiclassical spectrum is shown in Fig. 2(b). We show the quantitative agreement with ED in the Supplemental Material [22]. The LLs alternately broaden and pinch off at magic zeros, and the corresponding DOS divergences directly manifest as peaks in compressibility $dn/d\mu$ [see, e.g., Fig. 3(b) and the Supplemental Material [22]]. Importantly, we have placed no restrictions on V_0/ω_c, so our results are all orders in conventional perturbation theory. Moreover, our treatment did not depend on the precise energy dispersion, and a different dispersion would only alter geometric details such as Fermi surface areas and link phases. The existence of magic zeros, which is our main focus, is robust to all these details.

So far we have assumed the Fermi surface intersects only a single pair of Bragg planes at $\pm q\hat{\boldsymbol{x}}/2$. In moiré materials made of highly doped semiconductors or metals, however, $V(\boldsymbol{r})$ may have a small wave vector compared to the size of the Fermi surface, resulting in a network many overlaps. An important simplification is that the gaps at the intersections form a distinct hierarchy with $E_{\text{gap}}^{n\text{th}} \sim V_0^n/(v_F k_F)^{n-1}$ at an nth order Bragg plane. Therefore P has a double-exponential dependence on n and only a few crossings are active, with the rest completely avoided ($P = 0$) or trivial ($P = 1$). The simplest scenario is when only the intersections at the first-order Bragg plane are active. From Eq. (6), for the parabolic case this requires $V_0^4/(v_F k_F)^3 \ll \omega_c \sin\alpha_2$, $V_0^2/v_F k_F \ll \omega_c \sin\alpha_1$ where α_j is the intersection angle at the jth Bragg plane (and $\alpha_1 \approx \alpha_2$ when intersections are close together). In this "first-order regime" [42], the network model maps exactly back onto

the simplest case of a single intersection, Fig. 2(a). Therefore the DOS plot is the same as before, albeit with a slightly restricted regime of validity.

Let us discuss the extension to 2D potentials, such as a triangular lattice potential. Strictly speaking, the network model approach is only valid when φ, the number of flux quanta per real-space unit cell, is a rational number p/q; then the network unit cell is enlarged by a factor of p and each LL contains p subbands (for coprime p, q) [28]. However, if the enlarged unit cell consists of only original and lens orbits, they decouple when W becomes diagonal, and the flux at a magic zero can be approximated arbitrarily well by a rational φ. Thus magic zeros arise in this case with identical conditions. When the network topology has overlapping lens orbits, we conjecture that magic zeros still arise (see Supplemental Material [22]). For magic zeros to arise, the lens orbits of the network model must have equal areas, which requires wave vectors of equal magnitude. This is consistent with the perturbative result of Eq. (3).

We underscore a few necessary conditions for magic zeros which are frequently satisfied in moiré materials: (i) a superlattice potential consisting of equal-magnitude wave vectors must be present, (ii) the Fermi surface must be invariant under the rotational symmetry of the potential, and (iii) the potential is not so strong as to significantly restructure the band structure. Perturbations which would broaden magic zeros include higher order harmonics, strain, or anisotropic dispersions.

A natural question is whether TBG [43,44] exhibits magic zeros. While our theory based on a scalar moiré potential does not apply directly, we find magic zeros exist in the chiral limit [17] at *any* twist angle; we plot the noninteracting perturbative DOS and compressibility in Fig. 3 and include details in the Supplemental Material [22].

The flat Chern band at magic zeros provides an ideal setting for realizing fractional quantum Hall (FQH) states and other novel states at fractional fillings. For instance, the increased bandwidth away from magic zeros weakens the Laughlin state and may induce a transition into metallic states or electron crystals. We leave these directions to future work.

We thank Ray Ashoori and Long Ju for helpful discussions. This work is supported by the U.S. Department of Energy, Office of Science, Basic Energy Sciences, under Award No. DE-SC0020149 (N. P.), a Simons Investigator Award from the Simons Foundation (L. F.), and the STC Center for Integrated Quantum Materials (CIQM) under NSF Grant No. ECCS-2025158 (T. D. and P. C.). L. F. is partly supported by the David and Lucile Packard Foundation.

[*] These authors contributed equally to this work.

[1] D. J. Thouless, M. Kohmoto, M. P. Nightingale, and M. den Nijs, Phys. Rev. Lett. **49**, 405 (1982).
[2] P. G. Harper, Proc. Phys. Soc. London Sect. A **68**, 874 (1955).
[3] D. R. Hofstadter, Phys. Rev. B **14**, 2239 (1976).
[4] M. Wilkinson, Proc. R. Soc. A **391**, 305 (1984).
[5] R. Bistritzer and A. H. MacDonald, Phys. Rev. B **84**, 035440 (2011).
[6] Y. Li, S. Dietrich, C. Forsythe, T. Taniguchi, K. Watanabe, P. Moon, and C. R. Dean, Nat. Nanotechnol. **16**, 525 (2021).
[7] C. Forsythe, X. Zhou, K. Watanabe, T. Taniguchi, A. Pasupathy, P. Moon, M. Koshino, P. Kim, and C. R. Dean, Nat. Nanotechnol. **13**, 566 (2018).
[8] M. Drienovsky, J. Joachimsmeyer, A. Sandner, M.-H. Liu, T. Taniguchi, K. Watanabe, K. Richter, D. Weiss, and J. Eroms, Phys. Rev. Lett. **121**, 026806 (2018).
[9] R. Huber, M.-H. Liu, S.-C. Chen, M. Drienovsky, A. Sandner, K. Watanabe, T. Taniguchi, K. Richter, D. Weiss, and J. Eroms, Nano Lett. **20**, 8046 (2020).
[10] B. Hunt, J. D. Sanchez-Yamagishi, A. F. Young, M. Yankowitz, B. J. LeRoy, K. Watanabe, T. Taniguchi, P. Moon, M. Koshino, P. Jarillo-Herrero, and R. C. Ashoori, Science **340**, 1427 (2013).
[11] C. R. Dean, L. Wang, P. Maher, C. Forsythe, F. Ghahari, Y. Gao, J. Katoch, M. Ishigami, P. Moon, M. Koshino, T. Taniguchi, K. Watanabe, K. L. Shepard, J. Hone, and P. Kim, Nature (London) **497**, 598 (2013).
[12] Y. Okada, W. Zhou, C. Dhital, D. Walkup, Y. Ran, Z. Wang, S. D. Wilson, and V. Madhavan, Phys. Rev. Lett. **109**, 166407 (2012).
[13] E. M. Spanton, A. A. Zibrov, H. Zhou, T. Taniguchi, K. Watanabe, M. P. Zaletel, and A. F. Young, Science **360**, 62 (2018).
[14] B. Andrews and A. Soluyanov, Phys. Rev. B **101**, 235312 (2020).
[15] L. Onsager, Lond. Edinb. Dublin Philos. Mag. J. Sci. **43**, 1006 (1952).
[16] L. Ju, L. Wang, T. Cao, T. Taniguchi, K. Watanabe, S. G. Louie, F. Rana, J. Park, J. Hone, F. Wang, and P. L. McEuen, Science **358**, 907 (2017).
[17] G. Tarnopolsky, A. J. Kruchkov, and A. Vishwanath, Phys. Rev. Lett. **122**, 106405 (2019).
[18] D. Pfannkuche and R. R. Gerhardts, Phys. Rev. B **46**, 12606 (1992).
[19] C. Jin, E. C. Regan, A. Yan, M. Iqbal Bakti Utama, D. Wang, S. Zhao, Y. Qin, S. Yang, Z. Zheng, S. Shi, K. Watanabe, T. Taniguchi, S. Tongay, A. Zettl, and F. Wang, Nature (London) **567**, 76 (2019).
[20] M. Wilkinson, J. Phys. A **20**, 1761 (1987).
[21] R. Huber, M.-N. Steffen, M. Drienovsky, A. Sandner, K. Watanabe, T. Taniguchi, D. Pfannkuche, D. Weiss, and J. Eroms, arXiv:2106.11328.
[22] See Supplemental Material at http://link.aps.org/supplemental/10.1103/PhysRevLett.129.116804 for details about the wavefunctions, semiclassical model, application to TBG, and compressibility signatures.
[23] E. I. Blount, Phys. Rev. **126**, 1636 (1962).
[24] M. H. Cohen and L. M. Falicov, Phys. Rev. Lett. **7**, 231 (1961).
[25] J. R. Reitz, J. Phys. Chem. Solids **25**, 53 (1964).
[26] S. N. Shevchenko, S. Ashhab, and F. Nori, Phys. Rep. **492**, 1 (2010).
[27] A. B. Pippard, Proc. R. Soc. A **270**, 1 (1962).
[28] A. B. Pippard, Phil. Trans. R. Soc. A **256**, 317 (1964).
[29] Y.-Z. Chou, F. Wu, and S. Das Sarma, Phys. Rev. Research **2**, 033271 (2020).

[30] W. G. Chambers, Phys. Rev. **140**, A135 (1965).
[31] R. G. Chambers, Proc. Phys. Soc. London **88**, 701 (1966).
[32] M. Drienovsky, F.-X. Schrettenbrunner, A. Sandner, D. Weiss, J. Eroms, M.-H. Liu, F. Tkatschenko, and K. Richter, Phys. Rev. B **89**, 115421 (2014).
[33] D. Xiao, M.-C. Chang, and Q. Niu, Rev. Mod. Phys. **82**, 1959 (2010).
[34] J. B. Keller, Ann. Phys. (N.Y.) **4**, 180 (1958).
[35] G. P. Mikitik and Yu. V. Sharlai, Phys. Rev. Lett. **82**, 2147 (1999).
[36] J. N. Fuchs, F. Piéchon, M. O. Goerbig, and G. Montambaux, Eur. Phys. J. B **77**, 351 (2010).
[37] G. Szego, *Orthogonal Polynomials*, 4th ed., American Mathematical Society Colloquium Publications Vol. 23 (American Mathematical Society, Providence, 1975).
[38] R. R. Gerhardts, D. Weiss, and K. v. Klitzing, Phys. Rev. Lett. **62**, 1173 (1989).
[39] C. Zhang and R. R. Gerhardts, Phys. Rev. B **41**, 12850 (1990).
[40] P. Steda and A. H. MacDonald, Phys. Rev. B **41**, 11892 (1990).
[41] C. W. J. Beenakker, Phys. Rev. Lett. **62**, 2020 (1989).
[42] S. Spurrier and N. R. Cooper, Phys. Rev. B **100**, 081405(R) (2019).
[43] R. Bistritzer and A. H. MacDonald, Proc. Natl. Acad. Sci. U.S.A. **108**, 12233 (2011).
[44] Y. Cao, V. Fatemi, S. Fang, K. Watanabe, T. Taniguchi, E. Kaxiras, and P. Jarillo-Herrero, Nature (London) **556**, 43 (2018).

Correction: The omission of a support statement in the Acknowledgments has been fixed.